

Football Helmet: Head to Ground Test Device

Technical Team Members:

Dawson Chitwood, Aidan Connor, Lauren Gagermeier, William Moeller, Binh Nguyen,
Sam Suppes, Tristan Witz, and Max Wooten



May 2, 2025

TECHNICAL ADVISOR

Richard Kent, Department of Mechanical Engineering

Problem Statement

Our technical project seeks to develop a better system for the simulation of linear-rotational head-to-ground (H2G) impacts. With the rise in awareness of the dangers and pervasive impacts of concussions, especially in regards to American Football, helmet companies and the National Football League (NFL) have come to rely extensively on modeling and simulating real-world impact conditions to design safer helmet technologies. While considerable resources and research have gone into the production of institution-quality direct impacts on helmets, relatively little is known about the “whipping” impact, a phenomenon that is often seen in football (Kent, 2024). A direct impact can be described as a “strike” on the helmet, and would occur in the field of play most frequently as a head-to-head or head-to-body collision. A “whipping” impact is characterized by a rotational smacking of the head, and would occur in the field of play most frequently as a H2G impact, as depicted in Figure 1 below.

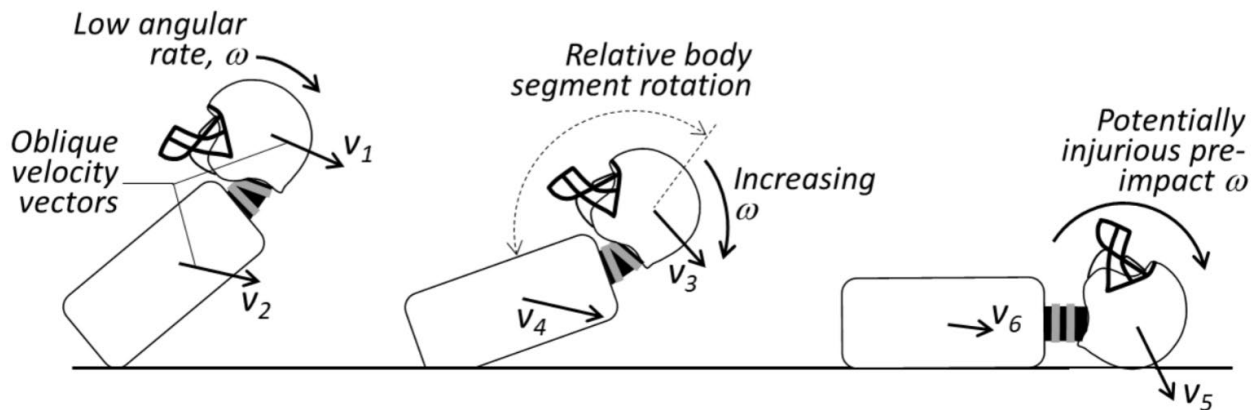


Figure 1: H2G “whipping” kinematic (Image source: Kent Head to Ground Test Device 2024)

Though these impacts have been only lightly studied, it is not due to a lack of application for the research. Almost 20% of concussions in the NFL are estimated to be caused by this sort of head-to-ground impact, and boosting helmet resistance to these impacts would serve to

meaningfully increase player protection (Kent et.al., 2019). Rather, the lack of research stems from the difficulty of simulation, and the massive variation in boundary conditions of these impacts. Angular velocity during time of impact covers a wide range in data collected from video capture of real world impact scenarios. Additionally, body and head angle at time of impact are two impactful, and independent, variables that also need to be analyzed.

Creating a model which can accurately cover the range of these initial impact conditions, while limiting error or chaos inherent to a moving impact system is a considerable design challenge. In order to control the impacts in favor of repeatable data, impact conditions must be constrained, which reduces the applicability of the simulation. Increasing the variability and accuracy of the impact introduces dynamic chaos which requires a high-level understanding of the force dynamics to tune out of the system. This equally reduces the applicability of a system intended for sale to a generic audience who may be unable to retrieve repeatable data from the system.

Research

Recent research efforts have focused on the critical assessment of football helmet performance H2G impacts. One such significant contribution is the paper entitled “The biomechanics of concussive helmet-to-ground impacts in the National Football League” by Kent et al. (2019). This comprehensive study addresses the urgent need for effective testing methodologies specifically tailored for H2G scenarios, which are responsible for a significant percentage of concussion in the sport of football. Unlike previous studies, which predominantly concentrated on helmet-to-helmet impacts, this paper hones in on the unique dynamics inherent to H2G impacts. The authors conducted an analysis of 16 incidents in which NFL players

sustained concussion due to H2G collisions, employing high-speed video analysis to capture details of the impact mechanics. The study quantified critical parameters, revealing “an average resultant closing velocity of 8.3 m/s at an angle close to 45 degrees and notable pre-impact angular velocities that reached as high as 54.1 rad/s.” (Kent et al., 2019, p. 2). This research is uniquely positioned as one of the only extensive analyses focusing on the specific biomechanics associated with H2G impacts.

In their innovative approach, Kent et al. (2019) utilized an anthropomorphic test device (ATD) designed to simulate realistic environmental conditions typical of football play. The study revealed essential characteristics of helmet interactions during H2G impacts, notably the decoupling effect between the helmet and the head. Their findings indicated that during impact, the head could rebound within the helmet, resulting in changes in both linear and angular motion greater than that of the helmet itself. The researchers also observed that the helmets exhibited a vertical rebound velocity averaging 24% greater than the vertical component of its initial closing velocity, which suggests that conventional testing methods may fail to replicate the true impact dynamics experienced during actual game play (Kent et al., 2019). These insights are pivotal, as they highlight the deficiencies in current helmet testing paradigms that often neglect the complexities of real-world H2G impacts. Kent et al.’s study serves as a crucial reference for ongoing research and development in helmet safety and protocol enhancement in professional football, signaling a transformative shift in research focus toward mitigating concussion risks associated with H2G impacts.

Building upon these foundational insights, Lessley et al. (2020) expanded the discourse on helmet safety by delving into position-specific circumstances surrounding H2G concussions in the NFL. Their work is particularly noteworthy as it correlates the biomechanics of H2G

impacts with the specific position of players on the field, thereby allowing for the design of helmets that cater to the unique needs of different player roles. By analyzing the circumstances under which concussion occurs, the authors advocate for the development of position-specific helmets that integrate advanced shock-absorbing technologies tailored to mitigate the risks associated with H2G impacts. This approach underscores the necessity of a nuanced understanding of how various positions are subjected to distinct impact dynamics, further enhancing the relevance of helmet safety measures. The research spotlighted specific impact directions that players experience according to their positions. This allows helmet engineers to consider factors such as placement of padding and the materials used in helmet construction, which could lead to breakthroughs in preventive helmet technology.

The research conducted by Kent et al. (2019) and Lessley et al. (2020) emphasizes the critical need for a H2G impact testing device that integrates biomechanical insights with effective engineering practices. Their findings reveal the complex dynamics of helmet impacts, highlighting the necessity for a device that accurately replicates various conditions encountered during gameplay to evaluate helmet performance reliably. In response to these insights, our initiative will focus on developing a simple yet practical testing device capable of simulating a range of impact scenarios.

Ideation

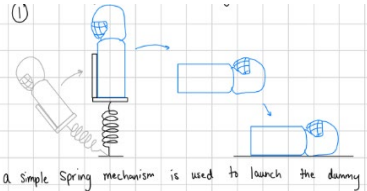
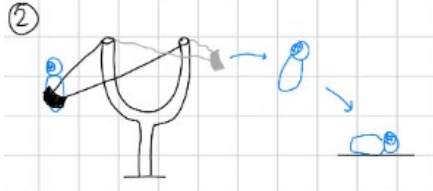

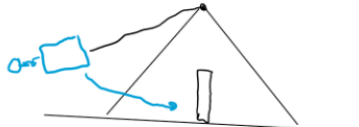
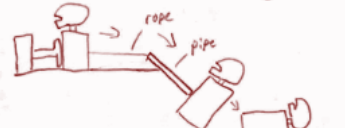

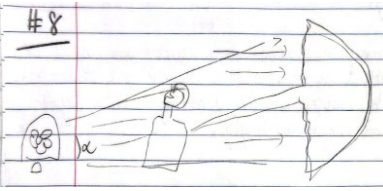
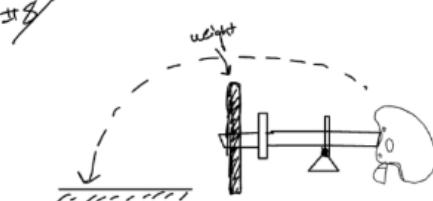
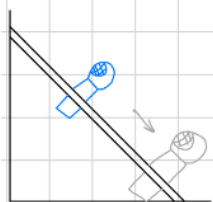
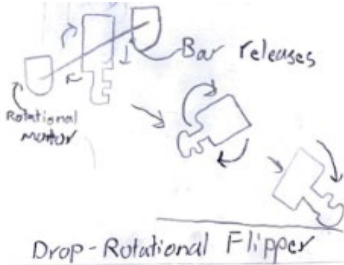
<p><u>Idea 1</u></p>  <p>A Simple Spring mechanism is used to launch the dummy</p>	<p><u>Idea 2</u></p>  <p>6. Linear impactor pushes dummy off ledge, but rope and pipe are attached to maintain a more consistent velocity vector as dummy falls.</p>	<p><u>Idea 3</u></p> 
<p><u>Idea 4</u></p> 	<p><u>Idea 5</u></p> 	<p><u>Idea 6</u></p>  <p>See-saw launcher dummy onto ground</p>
<p><u>Idea 7</u></p> 	<p><u>Idea 8</u></p>  <p>Barbell Seesaw</p>	<p><u>Idea 9</u></p>  <p>a beam is fixed at an adjustable angle and is suspended in the air. The dummy slides down the beam until it hits the floor</p>
<p><u>Idea 10</u></p>  <p>Drop-Rotational Flipper</p>		

Table 1: Ideations

After conducting a comprehensive analysis of the existing H2G model developed by Dr. Richard Kent and identifying its limitations, our team initiated the design process by generating ten preliminary concepts aimed at addressing the core challenges. These conceptual solutions were roughly sketched and systematically organized, as shown in Table 1.

Idea 1 involves attaching a spring mechanism to the base of the dummy, enabling it to rebound upon impact and fall back, thereby simulating the characteristic "whipping" motion. Idea 2 proposes the use of a slingshot to launch the dummy at a calculated trajectory, allowing it to fall in a manner that replicates natural impact dynamics. Idea 3 employs a magnetic vertical support that holds the dummy until a release mechanism is triggered, causing a controlled drop to the ground. Idea 4 draws inspiration from pendular motion: the dummy is suspended by a long string, and as it swings through the air, it strikes a fixed obstacle at a predetermined point to induce the whipping effect.

In contrast, Idea 5 takes a completely different approach by forgoing elevation altogether. Instead, the dummy is mounted horizontally on a linear impactor designed to deliver a direct force to the torso, effectively simulating the moment of contact during a football tackle. To ensure consistent velocity, a pulley system involving a rope and pipe is incorporated. Idea 6 introduces a creative seesaw mechanism, where placing an appropriate counterweight on one side propels the dummy on the opposite side into the air, culminating in a realistic fall.

Idea 7, while conceptually intriguing, presents significant practical challenges. It features a parachute-assisted launch, driven by a high-powered fan that provides lift. Once the dummy reaches a target altitude, the parachute is disengaged to allow a free fall. Ideas 8 and 10 share

similarities with the other elevated concepts, incorporating variations on controlled descent mechanisms.

Ultimately, Idea 9 emerged as the most viable solution due to its practical feasibility, ease of implementation, and design simplicity. In this configuration, a beam is installed at an adjustable incline and suspended above ground level, allowing the dummy to slide down and impact the surface below in a manner that accurately replicates the desired "whipping" kinematic.

Selection and Screening

Concept Selection	Initial Concept Variants									
Selection Criterion	1	2	3	4	5 (REF)	6	7	8	9	10
Variability of Impact	0	-	-	0	0	-	+	-	+	+
Repeatability of Test	-	-	+	0	0	-	-	+	+	-
Cost of Unit	+	+	-	-	0	+	-	-	0	-
Simplicity of Design	+	+	0	-	0	+	-	+	+	-
Boundary Conditions	-	-	0	+	0	-	0	-	0	+
Energy Usage	+	+	+	0	0	+	-	+	+	-
Ease of Testing Procedures	0	0	-	-	0	+	-	+	+	-
Pluses	3	3	2	1	0	4	1	4	5	2
Minuses	2	3	3	3	0	3	4	3	0	5
Net	1	0	-1	-2	0	1	-3	1	5	-3
Rank	2	5	7	8	5	2	9	2	1	9
Continue?	Yes	No	No	No	No	Yes	No	No	Yes	No

Table 2: Initial Concept Selection and Screening

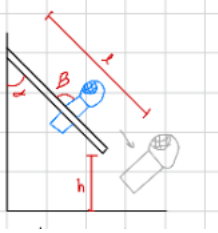
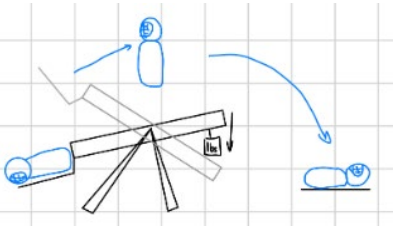

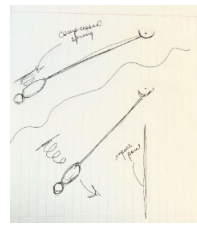
 <p><u>Idea A</u></p>	 <p><u>Idea B</u></p>
 <p><u>Idea C</u></p>	 <p><u>Idea D</u></p>

Table 3: Improved Concept Selection

Concept Selection		Improved Concept Variants							
Weight	Selection Criterion	Idea A	Score A	Idea B	Score B	Idea C	Score C	Idea D	Score D
25	Variability of Impact	0.9	22.5	0.6	15	0.5	12.5	0.7	17.5
15	Repeatability of Test	0.95	14.25	0.4	6	0.4	6	0.75	11.25
25	Cost of Unit	0.3	7.5	0.8	20	0.6	15	0.65	16.25
10	Simplicity of Design	0.95	9.5	0.8	8	0.75	7.5	0.8	8
15	Boundary Conditions	0.95	14.25	0.7	10.5	0.7	10.5	0.45	6.75
5	Energy Usage	1	5	1	5	1	5	1	5
5	Ease of Testing Procedures	0.85	4.25	0.5	2.5	0.5	2.5	0.65	3.25

	Net		77.25		67		59		68
	Rank		1		3		4		2
	Continue?	Yes		No		No		No	

Table 4: *Improved Concept Selection and Screening*

In the initial concept sorting with 10 aforementioned ideas, all of the 7 criteria were equally weighted (Table 2). Criteria were derived from initial design constraints, and planned application: Variability of Impact and Boundary Conditions were chosen to successfully simulate diverse concussion scenarios in the NFL. Repeatability of the test was considered to make sure all our testing data is consistent throughout different testing sessions. cost of unit, simplicity of design, energy usage, and ease of testing procedure were considered to satisfy the budget's constraints. The scoring system (positive, neutral, and negative) was used to quantitatively rank the initial designs, from which we moved forward with three concepts labeled as ideas 1, 6, and 9. To ensure a consistent evaluating process, our entire team collaboratively discussed and assessed each ideation in detail to align our assessments. This approach helped us to minimize biases and ensured a fair selection process, with all members contributing equally to the final ranking.

Incorporating strengths of the initial designs into designs 1, 6 and 9, four new design iterations were screened, labeled Idea A, B, C, and D in Table 3. This time, all criteria were weighted on importance. Variability of impact and cost of unit are the two most important criteria for our final testing design, which weigh up to 50% of total consideration. Repeatability of test and boundary conditions comprise up to 30% of our criteria, as those two considerations are essential for the real-world application of our device. Weights are noted in Table 4. Two key

criteria were advanced: The cost per unit which would govern the economic feasibility of the design, and the variability of impact, which was essential to modeling the broad range of naturally occurring helmet impact incidences. Other criteria of importance included repeatability, simplicity, and boundary conditions. After scoring the secondary round of designs following the exact same outlined procedure on this weighted scale, design A was chosen.

Specifications and Idea Development

Once an idea based on the general concept of our project was chosen, we established an initial set of specifications for the design. These specifications are as follows:

1. Product must correctly simulate linear and rotational velocity of a head to ground impact, by reaching target values of 8.0 m/s and 20.0 rad/s respectively.
2. Product must simulate ground impact in a repeatable manner. When an identical test is run we expect a standard deviation of less than a 2 for the pre-impact velocities.
3. Product must have a percent error of under 5% between theoretical and experimental values for the pre-impact velocities.
4. Product must be able to be reset in 5 minutes or less in order to provide ample opportunities for data collection by the consumer.
5. Product must be able to be operated by inexperienced and non-technically competent consumers (for example: Riddell, NFL testing) such that it is operable by those who have no background of impact science or design.
6. Product must be modifiable to provide a range of impact conditions. Adjusting release point and track angle will allow expected changes in measured numbers.

7. Product should be designed around commercially available systems, to regulate price and minimize manufacturing costs. Products should utilize cheap forms of energy (gravity, springs) to simulate large impacts.

Working on the initial design that was chosen through the ideation process, the specifics of the system were refined to meet the demands of the above specifications. Through research, testing, and simulation, we iterated on the initial design working to maximize the platform's performance to suit the above benchmarks.

One of the first areas of research we conducted was to obtain linear and angular pre-impact velocities of NFL players' heads in H2G concussion instances. We evaluated the tables shown below, which provide specific velocity values of NFL concussions instances.

Case	$(V_0)_{horiz}$ (m/s)	$(V_0)_{vert}$ (m/s)	$(V_0)_R$ (m/s)	α (deg)	ΔV_{horiz} (m/s)	ΔV_{vert} (m/s)
02	8.0	7.9	11.3	45.4	-5.3	-9.5
15	5.7	6.0	8.2	43.6	-2.7	-6.8
39	4.1	3.6	5.5	49.1	-2.3	-3.4
19	4.2	5.0	6.5	39.9	-2.0	-6.0
20	7.2	3.6	8.0	63.6	-2.4	-5.5
21	4.4	5.7	7.2	37.2	-3.3	-8.9
01	6.0	6.5	8.8	42.4	-2.3	-7.2
37	4.0	4.7	6.2	40.4	-2.3	-6.6
18	1.5	6.5	6.6	12.6	-4.5	-8.5
10	6.4	6.9	9.4	42.7	-0.3	-8.3
35	7.0	6.3	9.4	48.1	-3.3	-8.0
51	3.0	6.3	7.0	25.8	-2.5	-7.5
07	6.3	5.4	8.3	49.3	-6.0	-6.9
42	2.2	6.8	7.2	17.6	-0.8	-8.9
36	8.3	7.3	11.1	49.0	-3.5	-8.5
09	9.3	7.0	11.6	53.1	-6.6	-7.5
Mean	5.5	6.0	8.3	41.2	-3.1	-7.4
Median	5.8	6.3	8.1	43.1	-2.6	-7.5
Min	1.5	3.6	5.5	12.6	-6.6	-9.5
Max	9.3	7.9	11.6	63.6	-0.3	-3.4
S.D.	2.3	1.2	1.9	13.0	1.7	1.5
p^{\dagger}	0.26	0.17	0.22	0.39	0.31	0.47

[†] Heteroscedastic t-test, side vs. rear impact locations.

Table 5: Results of video analysis (field coordinate system), Kent et al. (2020)

	$(V_0)_x$	$(V_0)_y$	$(V_0)_z$	$(\omega_0)_x$	$(\omega_0)_y$	$(\omega_0)_z$	$(\omega_0)_R$	ΔV_x	ΔV_y	ΔV_z	ΔV_R	$\Delta \omega_x$	$\Delta \omega_y$	$\Delta \omega_z$	$\Delta \omega_R$
Case	(m/s)	(m/s)	(m/s)	rad/s	rad/s	rad/s	rad/s	(m/s)	(m/s)	(m/s)	(m/s)	rad/s	rad/s	rad/s	rad/s
02	-11.2	0.7	-1.2	3.8	53.8	3.3	54.1	8.6	-1.2	6.5	10.8	-1.0	-69.7	-1.9	69.7
15	-8.0	1.8	0.2	0.2	9.3	3.1	9.8	4.3	-2.2	5.5	7.3	-1.8	-35.6	-16.0	39.1
39	5.0	1.9	-1.2	2.2	-1.2	3.8	4.5	-3.7	-1.2	1.1	4.0	-2.9	-17.3	-8.7	19.6
19	-5.6	3.0	-1.4	0.2	4.1	3.5	5.4	6.2	-1.0	-0.3	6.3	-1.3	-14.6	-12.3	19.1
20	-4.6	4.2	5.1	4.0	-1.5	2.6	5.0	2.8	-5.1	1.1	6.0	-22.8	-9.7	-12.5	27.7
21	-3.6	6.2	0.1	3.5	3.7	9.7	11.0	7.7	-4.7	3.0	9.5	-2.1	-14.0	-24.2	28.1
01	5.4	6.4	-2.8	11.4	-6.1	6.0	14.3	-3.9	-5.7	3.0	7.5	-6.2	1.4	-3.3	7.1
37	1.3	6.0	-0.5	5.3	-6.0	6.3	10.2	1.2	-6.8	1.2	7.0	-10.3	-1.7	-15.2	18.4
18	-1.5	6.5	-0.1	6.3	0.7	3.4	7.1	4.4	-8.4	1.7	9.7	-8.7	6.0	-0.1	10.6
10	-8.7	0.4	3.4	4.6	23.9	8.1	25.7	8.0	-2.0	1.1	8.3	-10.2	-47.4	-16.2	51.1
35	-5.7	7.5	0.4	2.3	7.6	3.9	8.8	0.7	-8.3	-2.2	8.6	-18.0	5.4	-51.7	55.0
51	-6.4	1.9	1.9	0.4	7.7	0.4	7.8	7.8	-0.5	1.3	7.9	-0.4	-16.5	-2.5	16.7
07	6.1	5.2	-2.0	5.7	2.0	6.1	8.6	-7.7	-4.8	1.3	9.2	-8.5	3.9	-11.6	14.9
42	3.0	6.4	0.9	9.8	-4.5	6.3	12.5	-2.0	-8.5	1.8	8.9	-1.0	0.1	-20.5	20.5
36	3.4	9.4	-4.7	12.6	-8.5	7.8	17.1	2.3	-6.5	6.1	9.2	-14.0	-13.1	-15.7	24.8
09	3.9	10.9	0.9	13.4	-1.7	4.0	14.1	3.9	-8.9	2.3	10.0	-10.7	26.7	-11.4	30.9
Mean	-1.7	4.9	-0.1	5.3	5.2	4.9	13.5	2.5	-4.8	2.2	8.1	-7.5	-12.3	-14.0	28.3
Median	-2.6	5.6	0.0	4.3	1.4	3.9	10.0	3.4	-5.0	1.5	8.5	-7.4	-11.4	-12.4	22.6
Min	-11.2	0.4	-4.7	0.2	-8.5	0.4	4.5	-7.7	-8.9	-2.2	4.0	-22.8	-69.7	-51.7	7.1
Max	6.1	10.9	5.1	13.4	53.8	9.7	54.1	8.6	-0.5	6.5	10.8	-0.4	26.7	-0.1	69.7
S.D.	5.7	3.1	2.3	4.3	15.2	2.4	12.0	4.9	3.0	2.3	1.7	6.7	23.1	12.1	17.3
p^{\dagger}	<0.01	<0.01	0.21	<0.01	0.02	0.05	0.18	0.01	0.01	0.39	0.42	0.17	0.03	0.32	0.02

[†] Heteroscedastic t-test, side vs. rear impact locations.

Table 6: Results of video analysis (helmet coordinate system), Kent et al. (2020)

To summarize Tables 5 and 6, resultant linear velocity ranged from 5.5 to 11.6 m/s, and angular velocities ranged from 4.5 to 54.1 rad/s (Kent, 2020). After meeting with our technical advisor to discuss these numbers, target velocities of 8 m/s (resultant linear) and 20 rad/s (angular) were chosen as proof of concept parameters. These were the target velocities mentioned in specification 1.

Gravity was chosen as the driving force for the velocity components, as it provided perfectly repeatable, and cheap energy (specifications 2 and 7), minimizing simulation chaos and utility costs. This can be seen in Figure 2 below.

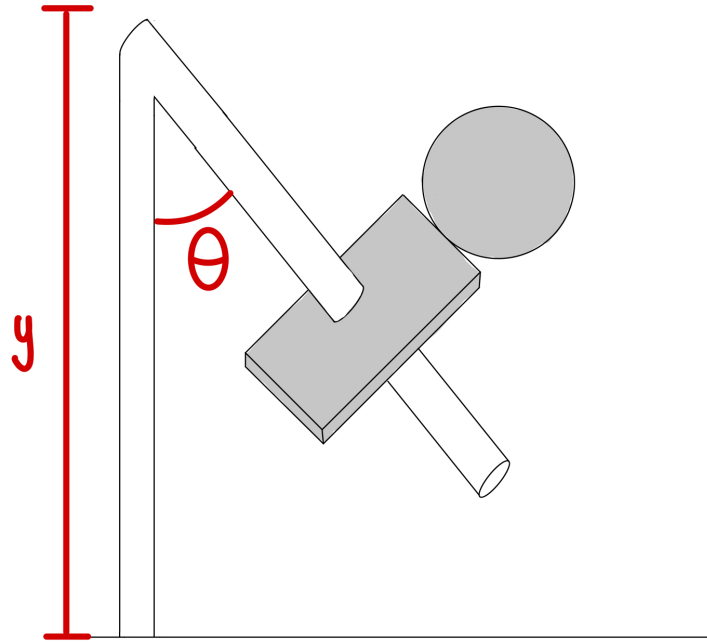


Figure 2: *Initial Design*

The dummy slides down the track only due to the force of gravity. As gravity provides a constant acceleration, using it as our driving force will limit our error when running identical tests. The initial design displays a hole through the middle of the dummy that allows it to slide down a pipe, eventually being released and hitting the ground.

After further consideration, to ensure repeatability we decided it was best to use track and carriages instead of a hole through the middle. We will use a two-track system with the dummy placed between the tracks to prevent rotation after release. The dummy will be tightly secured to the carriages, limiting any potential error and rotation caused by wobbling of the dummy as it slides down the track. The angle at which the dummy is secured relative to the ground will be precise and consistent across identical trials. The carriages, containing cam roller wheels, will run along the tracks with minimal friction, ensuring repeatability.

As identified in the ideation section, the variability of pre-impact velocities (specification 6) is the most important specification. Our initial design included an adjustable release height and track angle to create a range of pre-impact conditions. To determine this range we used the energy conservation equations seen in equations (1) and (2).

$$m * g * y = (1/2) * m * v_R^2 \quad (1)$$

Solved for resultant velocity:

$$v_R = \sqrt{2 * g * y} \quad (2)$$

Where m is mass of dummy, g is acceleration due to gravity, y is total height of track, and v_R is resultant velocity. From this resultant velocity, we can solve for the components of velocity

$$v_H = v_R * \sin(\theta) \quad (3)$$

$$v_V = v_R * \cos(\theta) \quad (4)$$

Where v_H is horizontal velocity, v_V is vertical velocity, and θ is the angle between the track and vertical. Based on these equations we determined we would need a track height of 3.26m to achieve our target resultant velocity, this calculation is shown in Appendix C. With this track height we determined our range of component velocities using equations 3 and 4, and this range can be visualized in Figure 3.

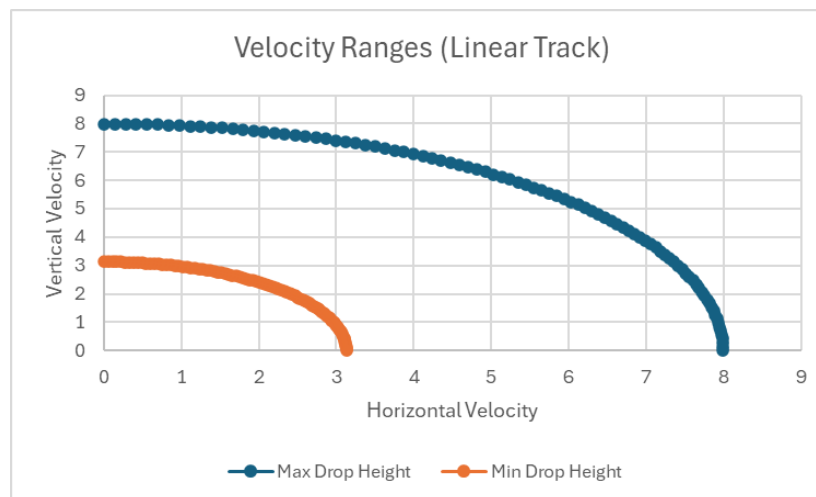


Figure 3: *Range of Velocities with Linear Track*

In the graph, the two lines represent all of the velocity components that can be hit from the maximum and minimum drop height at every different θ value. From this graph we realized that our range is restricted based on the relationship between the velocity components and the angle of the track as well as length of track. To expand our range, we decided to switch to a curved track which allows us to control the vertical and horizontal velocity components independently and hit a larger range of velocities. In addition, to limit the height of the track, we added a constant-force or “negator” spring to increase the horizontal velocity component. For the new track we will maintain the angled track-dummy contact points as used previously for the linear track.

The final design with the curved track and negator spring can be seen in Figure 4. When the dummy is on the track its potential energy will be converted to horizontal velocity, and when the dummy exits the rail apparatus the remaining potential energy (due to gravity) will be converted to vertical velocity. The constant force spring extends from a dowel near the base of the stand to a hook on the dummy. This increased potential energy will increase the pre-impact horizontal velocity.

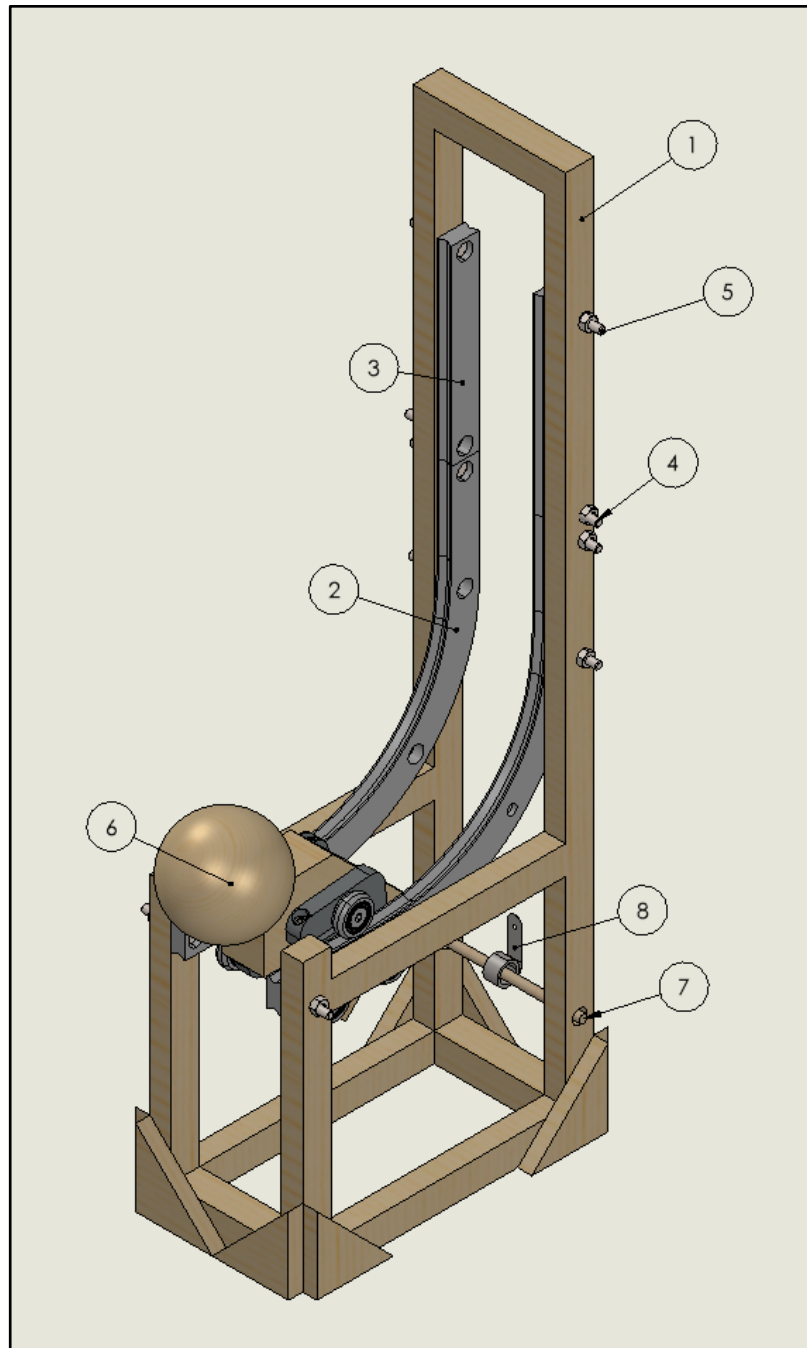


Figure 4: *Final Design*

Because of the change in design, we had new equations that governed theoretical pre-impact velocities. To calculate the pre-impact vertical velocity, we focused on the drop height (d in Figure 5) which measures the distance traveled by the head from the edge of the track to the moment the body hits the ground. Due to the perfectly horizontal release of the dummy off of the

track, we were still able to use Equation (2) to calculate our pre-impact vertical velocity.

However we replaced the height variable y with drop height d , and resultant velocity variable v_R with v_V which represents the vertical pre-impact velocity.

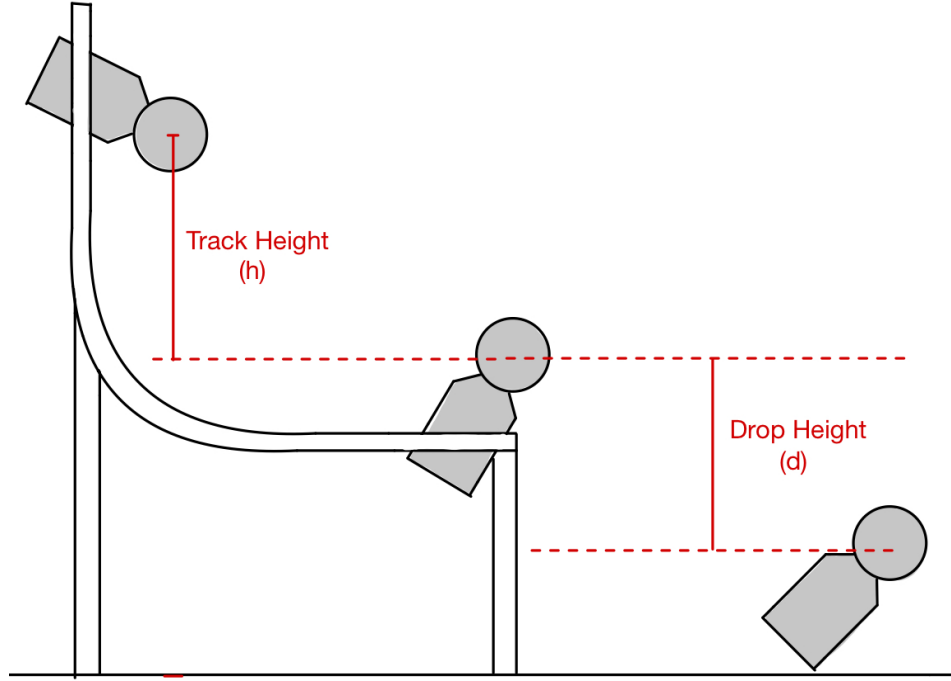


Figure 5: *Track vs Drop Height Dimension Model*

To calculate the horizontal pre-impact velocity, we used the following energy conservation equation:

$$(1/2) * m * v_H^2 = (F * x) + (m * g * h) \quad (7)$$

Solved for horizontal velocity:

$$v_H = \sqrt{\frac{2}{m}((F * x) + (m * g * h))} \quad (8)$$

Where F is the force provided by the negator spring, x is the length that the spring is displaced, and h is the height that the dummy starts at on the track, to the height of the dummy as it leaves the track (also referred to as the “track height” displayed in Figure 5. Equation (8) was

used to solve for the horizontal component of the pre-impact velocity throughout the rest of our design process.

Once both the vertical and horizontal pre-impact components were found, we were able to calculate the resultant velocity with the following equation:

$$v_R = \sqrt{v_H^2 + v_V^2} \quad (9)$$

Where v_R is the resultant velocity, v_H is the horizontal velocity, and v_V is the vertical velocity. Achieving a resultant velocity within our target range is one of the key components of our device (specification 1).

Due to the financial constraints on this project we decided to make a scaled model of our design as a proof of concept. The size of the scaled model was based on the materials that were available within our budget. This led us to try to initially achieve smaller target velocities, both linear and angular, which would increase in a full scale model. This full scale model would include a larger track size and more powerful springs, to achieve the NFL field reconstruction values. In order to scale the device down, the track, the spring, and the dummy dimensions were all scaled down based on available products. Using the equations above we were able to ensure that the new track hits the maximum velocity numbers that were specified as proof of concept parameters, with improved range variability.

In order to determine the angular velocity of our scaled design, we used a dynamic simulation in Solidworks. Depicted below in Figure 6, is a graph showing the resulting angular velocities, as well as the modeled dummy.

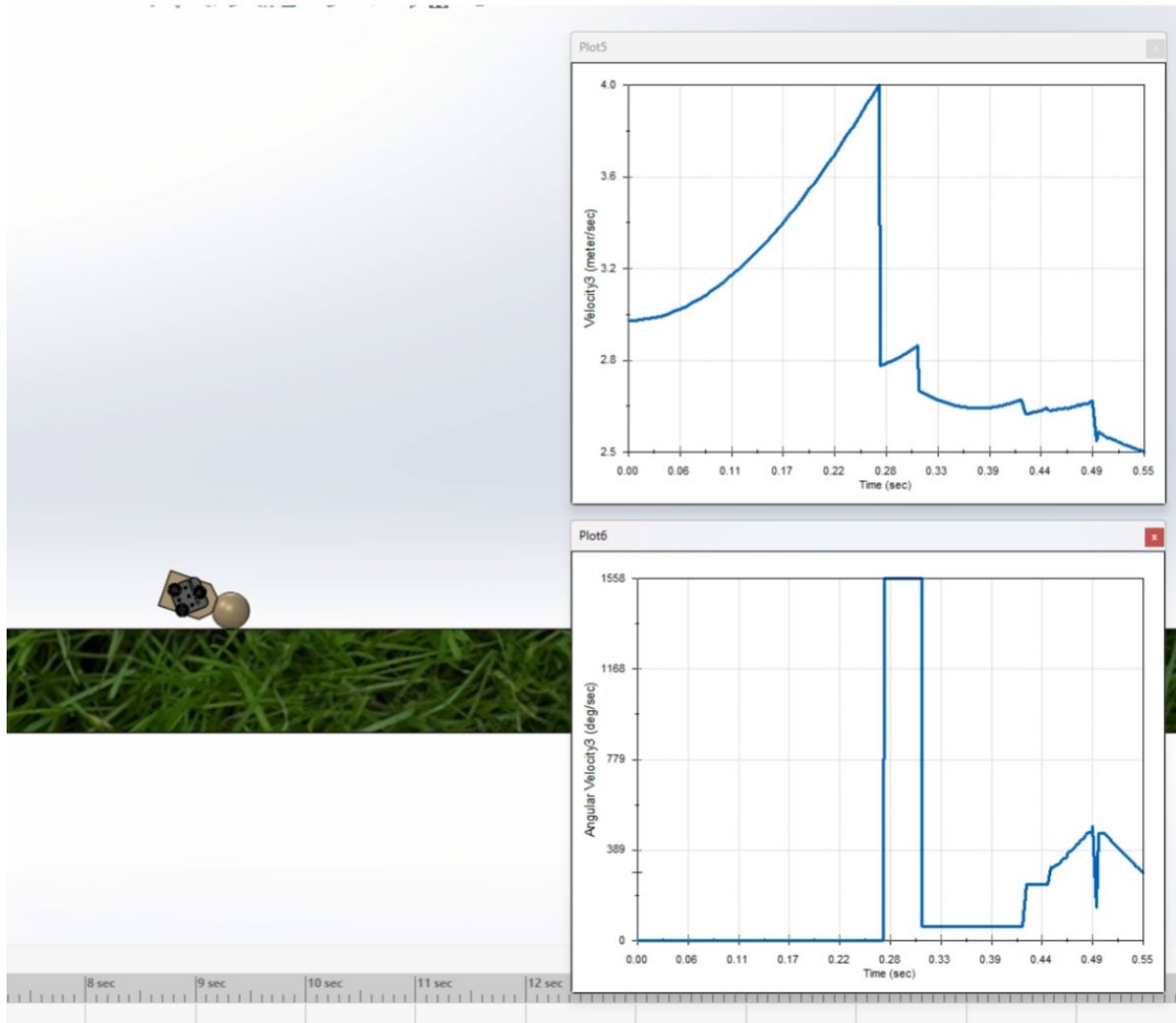


Figure 6: *Angular Velocities of Modeled Dummy*

Through many simulations similar to the one seen above, we were able to reach a range of rotational velocities from 5 to 30 rad/s. The simulation used initial conditions of the dummy based on calculated linear velocities. The impact surface was modeled to resemble field turf in both friction and restitution coefficients. The dummy's angle with the ground and dimensions were initially variable to determine the optimal realistic combination for impact angular velocity. After inputting these known initial and boundary conditions and running these simulations, our

resulting data supported the conclusion that our model should provide the target range of experimental values. After conducting this research and technical analysis, we established a final set of specifications that our design will accomplish. These specifications are as follows:

1. Product must correctly simulate ideal linear and rotational velocity ranges of a head to ground impact. The target linear resultant velocity range is 2.5 to 9 m/s, and the target rotational velocity range is 5 to 30 rad/s.
2. Product must be able to independently control the horizontal and vertical velocity in order to increase the variability of testing and replicate specific concussion instances.
3. Product must simulate ground impact in a repeatable manner. When an identical test is run we expect a standard deviation of less than a 2 for the pre-impact velocities.
4. Product must have a percent error of under 5% between theoretical and experimental values for the pre-impact velocities.
5. Products must be able to be reset in 5 minutes or less in order to provide ample opportunities for data collection by the consumer.
6. Product must be able to be operated by inexperienced and non-technically competent consumers (for example: Riddell, NFL testing) such that it is operable by those who have no background of impact science or design.
7. Product should be designed around commercially available systems, to regulate price and minimize manufacturing costs. Products should utilize cheap forms of energy (gravity, springs) to simulate large impacts.

Testing

All of our testing occurred on an outdoor turf football field to simulate NFL H2G impacts as closely as possible. In order to test our device we first had to take certain measures to ensure we were set up properly to record and analyze data regarding the dummy's movements. To do this, we set up three key testing features. The first was a tape measure. We set up a tape measure in line with the dummy's path of motion to use as a calibration distance for our video analysis. The next feature was the addition of distance markers along the vertical edge of the track. We made five different marks along the upper section of the track, starting from the very top and declining 50.8 mm every time. The purpose of these markers was to provide consistent initial releasing points for our trials. The last feature was setting up two iPhones on tripods to record the dummy's motion. The first iPhone was set up in line with the height of the bottom of the track. It was used to track the dummy's linear motion starting when the dummy launched from the track and ending at the initial point of contact with the ground. The next iPhone was set up at the point of the dummy's impact with the ground. It was used to track the head's angular velocity from the moment the body made contact with the ground through the moment the head made contact with the ground after experiencing the desired "whipping" effect. Once these three features were in place, we then developed a routine for each test. Figure 7 provides a visual of our testing set up.



Figure 7: *Test System*

Our testing routine consisted of three main practices to maintain repeatability and consistency. The first practice was properly lubricating the track and carriage bearings every three trials. This allowed us to keep friction to a minimum between the bearings and track. The second practice was to have someone inspect the release height of the dummy before it was set in motion, to ensure that it was being held at the same level as the marker we wanted it to be in line with. This practice promoted a repeatable track height which allows for more consistency among tests. The last practice was to run a trial at each height without video analysis to mark where the dummy would land, so our cameras could be placed in the proper position to document the dummy's motion. Once the cameras were in position, the tripod would be kept in the same spot until a new initial track height was used. With all of these measures in place, we were then able

to go about completing our testing matrix in a repeatable fashion in order to collect data regarding the dummy's linear and rotational velocities.

Our main test matrix had three variables that would affect each test: the track height, the drop height, and the constant-force spring being used (track and drop heights are described in Figure 5, force of each negator spring was provided by the manufacturer). We performed tests at five different track heights: 410 mm, 359.2 mm, 308.4 mm, 257.6 mm, and 206.8 mm. We performed tests at two different drop heights: 0.157 m and 0.406 m. Lastly, there were three different constant force springs used in our tests: 14.63 N, 30.60 N, and 47.15 N. Tests were also performed without a spring as well (0 N). Table 7 below shows a snapshot of how our data was organized.

Test Number	Spring Strength (lbs)	Spring Strength (N)	Drop Height (m)	Track Height (mm)	Image number	Rotational Image number	X velo	Y velo	Rotational velo	V	Avg V	Mean Rotation
31	3.29	14.63392	0.157	410	3491	5562	4.056	2.34	27.27	4.68		
32	3.29	14.63392	0.157	410	3492	5563	3.996	2.17	23.17	4.55		
33	3.29	14.63392	0.157	410	3493	5564	4.24	2.18	22.75	4.77	4.67	24.396666
34	3.29	14.63392	0.157	359.2	3495	5566	3.654	2.412	20.37	4.38		
35	3.29	14.63392	0.157	359.2	3496	5567	3.774	2.508	23.16	4.53		
36	3.29	14.63392	0.157	359.2	3497	5568	3.72	2.664	24.71	4.58	4.50	22.746666
37	3.29	14.63392	0.157	308.4	3498	5569	3.24	2.316	21.070	3.98		
38	3.29	14.63392	0.157	308.4	3499	5570	3.426	2.52	22.54	4.25		
39	3.29	14.63392	0.157	308.4	3500	5571	3.426	2.42	20.020	4.19	4.14	21.210
40	3.29	14.63392	0.157	257.6	3501	5572	3.066	2.472	24.01	3.94		
41	3.29	14.63392	0.157	257.6	3503	5574	3.216	2.404	20.51	4.02		
42	3.29	14.63392	0.157	257.6	3504	5575	2.904	2.184	21.77	3.63	3.86	22.096666
43	3.29	14.63392	0.157	206.8	3505	5576	2.68	2.58	19.11	3.72		
44	3.29	14.63392	0.157	206.8	3506	5577	2.538	2.124	16.38	3.31		
45	3.29	14.63392	0.157	206.8	3507	5578	2.706	2.4	19.25	3.62	3.46	18.246666
46	6.88	30.60224	0.157	410	3508	5579	4.638	2.16	25.1	5.12		
47	6.88	30.60224	0.157	410	3509	5580	4.776	1.944	24.9	5.16		
48	6.88	30.60224	0.157	410	3510	5581	5.06	2.496	26.4	5.64	5.30	25.466666
49	6.88	30.60224	0.157	359.2	3511	5582	4.5	2.424	28.9	5.11		
50	6.88	30.60224	0.157	359.2	3512	5583	4.818	2.436	27.8	5.40		
51	6.88	30.60224	0.157	359.2	3513	5584	4.596	2.496	24.2	5.23	5.25	26.966666
52	6.88	30.60224	0.157	308.4	3514	5585	4.332	2.448	16.31	4.98		
53	6.88	30.60224	0.157	308.4	3515	5586	4.104	2.124	14.98	4.62		
54	6.88	30.60224	0.157	308.4	3516	5587	4.098	2.22	16.94	4.66	4.75	16.076666
55	6.88	30.60224	0.157	257.6	3517	5588	3.924	2.376	15.89	4.59		
56	6.88	30.60224	0.157	257.6	3518	5589	3.732	2.088	15.54	4.28		
57	6.88	30.60224	0.157	257.6	3519	5590	3.858	2.328	14.35	4.51	4.46	15.26
58	6.88	30.60224	0.157	206.8	3520	5591	3.606	2.448	14.84	4.36		
59	6.88	30.60224	0.157	206.8	3521	5592	3.588	2.364	12.95	4.30		
60	6.88	30.60224	0.157	206.8	3522	5593	3.516	2.484	14.21	4.30	4.32	14

Table 7: Test Matrix Snapshot

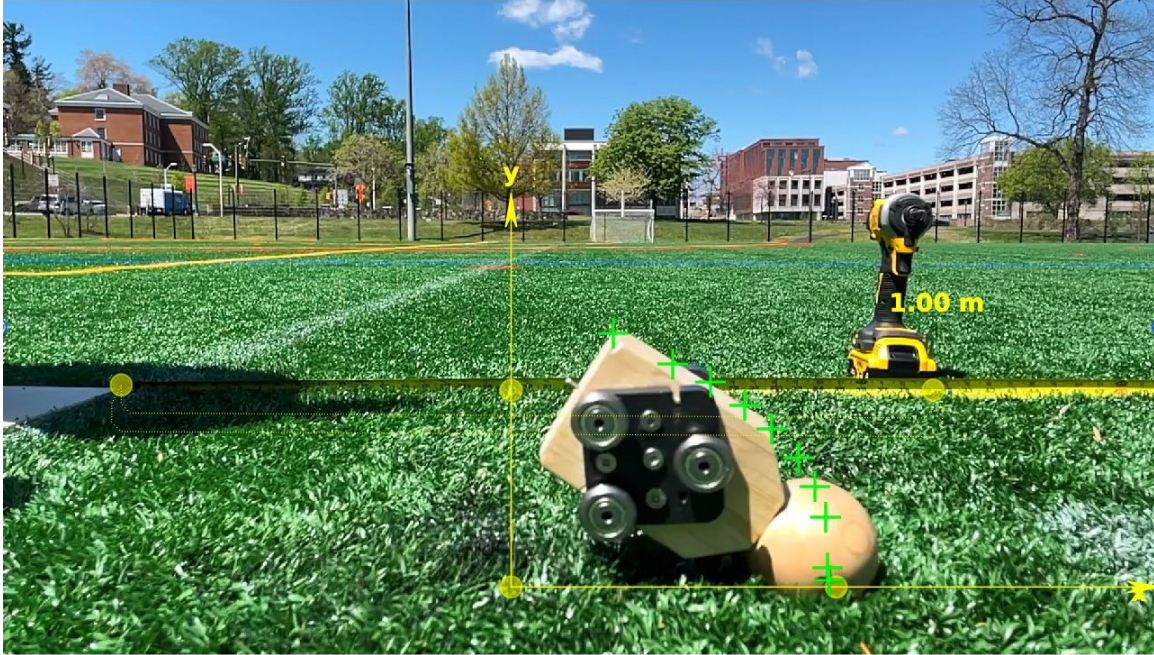


Figure 9: *Rotational Data-Tracking Through Capstone*

As data points were collected on PASCO Capstone, we entered them into our results matrix which can be seen in Appendix D. In order to summarize our results we developed a graph seen in Figure 10.

Pre-Impact Rotational Velocities and Impact Linear Velocity Magnitude

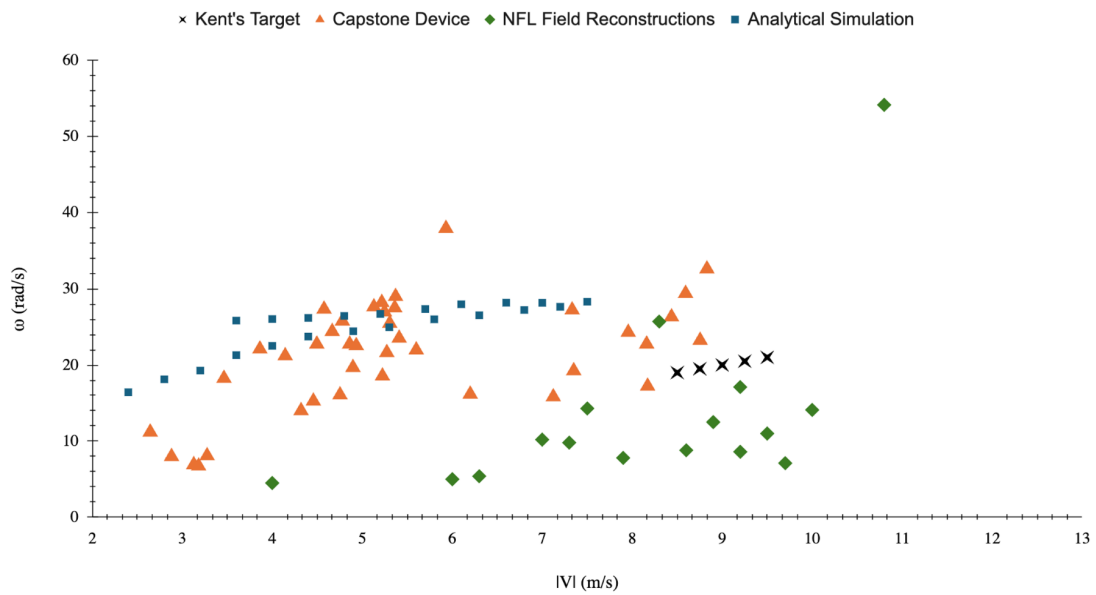


Figure 10: *Final Results*

In the graph, the y-axis represents angular velocity and the x-axis represents resultant velocity. The orange triangles on the graph display all of the data points our device hit. The angular velocities were obtained using PASCO video analysis, and the resultant velocities were calculated using Equation (9). This graph was the goal of our project, as we compared our results to NFL field reconstructions and our analytical simulation. Our device was able to cover a wide range of concussion instances with a downward scaled velocity. Our device also performed well in comparison to our analytical values (blue squares in Figure 10), however we did encounter errors during the testing process.

To determine the accuracy and precision of our device, we tracked error in two ways. The first was by comparing the experimental velocities to the theoretical values previously calculated using Equations (2) and (8). Percent error was calculated for every recorded velocity using the following equation:

$$\delta = \left| \frac{v_A - v_E}{v_E} \right| \cdot 100\% \quad (10)$$

Where δ is percent error, v_A is the actual velocity achieved, and v_E is the experimental velocity achieved. We averaged the percentages for trials of the same conditions. This would test the accuracy of our model to predict our device's behavior.

The percent errors of the horizontal velocities were promising. As seen in Figure 11 below, most percentages were below 10%, many being less than 5%. The most error was seen in trials that did not include a spring force. This is likely due to the friction force (which was ignored in our models) having a greater impact at lower velocities.

Spring Force (N)	Track Height (mm)	Average X Percent Error (%)
0	410	-14.18
	359.2	-12.23
	308.4	-14.55
	257.6	-16.46
	206.8	-19.77
14.6	410	1.98
	359.2	-1.18
	308.4	-3.46
	257.6	-3.85
	206.8	-8.11
30.6	410	-1.59
	359.2	0.62
	308.4	-5.39
	257.6	-4.20
	206.8	0.07
47.1	410	-10.09
	359.2	-6.90
	308.4	-7.46
	257.6	-4.70
	206.8	-5.86

Spring Force (N)	Average X Percent Error (%)
0	-6.5226
14.6	1.7199
30.6	-1.8535
47.1	-4.7795

Drop Height: 0.157 m

Drop Height: 0.406 m

Figure 11: *Average Percent Errors of Horizontal Velocities*

The percent errors of the vertical velocities proved to be much higher (shown below in Figure 12). There are a few potential reasons for these results. The first factor was that there was some rotation of the dummy body before it reached the ground. This caused the angle of impact to be different from the starting angle, thus increasing the vertical distance (drop height) the dummy head moved. Because our theoretical vertical velocity was calculated using a lower expected drop height, the perceived velocity was higher. Another potential factor is some deflection in the wood frame could have caused the release of the body to be at a very slight downward angle, giving a starting boost to the downward velocity as opposed to the theoretical perfectly horizontal launch.

Spring Force (N)	Track Height (mm)	Average Y Percent Error (%)
0	410	27.06
	359.2	44.04
	308.4	37.81
	257.6	34.09
	206.8	25.92
14.6	410	39.71
	359.2	29.00
	308.4	29.00
	257.6	38.57
	206.8	34.92
30.6	410	24.89
	359.2	23.30
	308.4	31.96
	257.6	24.44
	206.8	19.20
47.1	410	33.10
	359.2	8.94
	308.4	12.13
	257.6	12.59
	206.8	25.65

Spring Force (N)	Average Y Percent Error (%)
0	13.9761
14.6	7.8565
30.6	8.1115
47.1	-0.1328

Drop Height: 0.157 m Drop Height: 0.406 m

Figure 12: *Average Percent Errors of Vertical Velocities*

The second way we recorded error was by calculating the average standard deviation of every test condition combination. We determined the amount of variation seen between trials of the same parameters using the following equation:

$$\sigma = \sqrt{\frac{\sum (x_i - \mu)^2}{N}} \quad (11)$$

Where σ is the population standard deviation, Σ indicates taking the sum, x_i is each value from the population, μ is the population mean, and N is the size of the population. This data would be used to analyze the repeatability of our device. Our results indicate extremely repeatable trials, as our average standard deviations are all less than 0.4 m/s, as seen in Figure 13.

Spring Force	Track Height (mm)	Average Resultant Velocity Standard Deviation (m/s)
0 N	410	0.0548
	359.2	0.0772
	308.4	0.1754
	257.6	0.1914
	206.8	0.1301
14.6 N	410	0.1112
	359.2	0.1035
	308.4	0.1422
	257.6	0.2018
	206.8	0.2174
30.6 N	410	0.3434
	359.2	0.1193
	308.4	0.0280
	257.6	0.1623
	206.8	0.0058
47.1 N	410	0.3648
	359.2	0.1082
	308.4	0.1550
	257.6	0.0126
	206.8	0.0568

Drop Height: 0.157 m

Figure 13: *Average Standard Deviations of Resultant Velocities*

The device uses a combination of gravitational and spring-force energy to achieve the desired impact velocities and rotation. Energy conservation laws were used to calculate theoretical impact velocity, as described earlier in the specifications section. This data was used to create theoretical limits of the impact conditions the device should be able to achieve. The goal, with limited time for repeated testing, was to collect consistent results, to support the applicability of the device in the real-world.

Our testing data supported our theoretical calculations. As can be seen in Figure 10, our results achieve a range that is consistent with theoretical values.

Our initial testing points indicate very high rotational impact velocities corresponding to lower than expected linear velocity. We hypothesize that this is a result of only testing the dummy when aligned at 45 degrees to the ground. In order to achieve the full range of desired and theoretically achievable impact conditions, it is necessary to recreate high linear velocity impacts while sustaining low rotational velocity.

As mentioned in the initial specifications section, our device demonstrates a proof of concept that would allow helmet companies to use our design to create a larger, full-scale device to reach pre-impact velocities that align better with field reconstruction velocities listed in Kent's paper (Kent et al., 2020). Our device successfully showed that this type of device (when built full scale), could hit a wide range of pre-impact velocities that occur in NFL concussion instances. Our device, as expected, produced smaller pre-impact x and y velocities than most of the field reconstruction velocities. This can be shown in the chart below by the Capstone Device (black x's) resultant velocities ($|V|$) being smaller than most of the NFL Field Reconstructions (orange triangles).

Pre-Impact Rotational Velocities and Impact Linear Velocity Magnitude

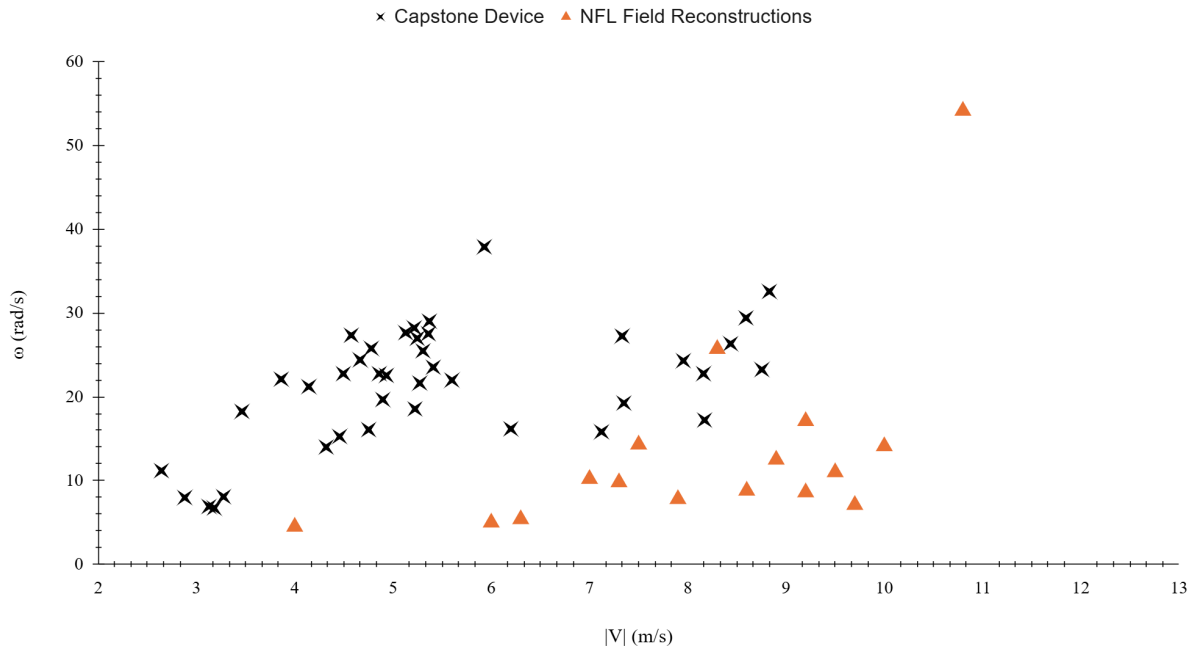


Figure 14: *Pre-Impact Rotational Velocities and Impact Linear Velocity Magnitude with Scaled Model*

Our tested data covers a range of net linear impact velocities $2.5 \text{ m/s} < |V| < 6.36 \text{ m/s}$, and rotational impact velocities $10.01 \text{ rad/s} < \omega < 44.8 \text{ rad/s}$, both of which fell well short of the range of desired field reconstruction velocity targets. The data does, however, reinforce our theoretical range that was predicted by the energy calculations used when designing the device. This provides strong support for our mathematical model of the launching process, and resulting impact velocities. Because of the empirical evidence supporting our model, we feel confident in making predictions surrounding a fully-scaled device, something more akin to the commercial application it is designed for. Our model supports a fully scaled model successfully hitting even the most extreme field reconstruction impact conditions. The clearest example of this is the outlier to the real world data, the only point with a resultant velocity $|V| > 11 \text{ m/s}$, or a rotational

velocity $\omega > 30$ rad/s. To reach these pre-impact velocity conditions a significantly larger device would need to be made, but our model shows its feasibility using the current design.

There are four factors of our design that have an effect on the pre-impact $|V|$, and ω . These factors are: (1) dummy mass, (2) spring force, (3) track height, and (4) drop height. The independent variation of these factors that is possible through the design allows for practically endless combinations of initial conditions that would allow our design to reach the full range of values between the largest and smallest plausible impact conditions. Having demonstrated through a scaled model the lower bound of impact conditions, we believe that by theoretically demonstrating our ability to hit the upper bound of impact conditions, we can show the full range of plausible impact conditions. To simulate the upper impact condition, the factors are as follows:

1. Dummy mass: 53 kilograms. This is the average weight of the head and torso of an NFL football player.
2. Spring force: 182.38 newtons. This is an example of a stronger constant-force spring you can buy from McMaster Carr. It only costs \$45 so would be extremely affordable (especially with an increased budget).
3. Track height: 2.5 meters.
4. Drop height: 2.5 meters.

These factors were calculated using the theoretical equations that accurately predicted the pre-impact horizontal and vertical velocities. The chart below shows the updated range of velocities that the full-scale device would be able to reach. This chart only includes the empirical data that we have already collected, scaled using larger conditions and with a more powerful spring. Notice how the entire range of NFL Field Reconstruction resultant velocities can be met.

Pre-Impact Rotational Velocities and Impact Linear Velocity Magnitude

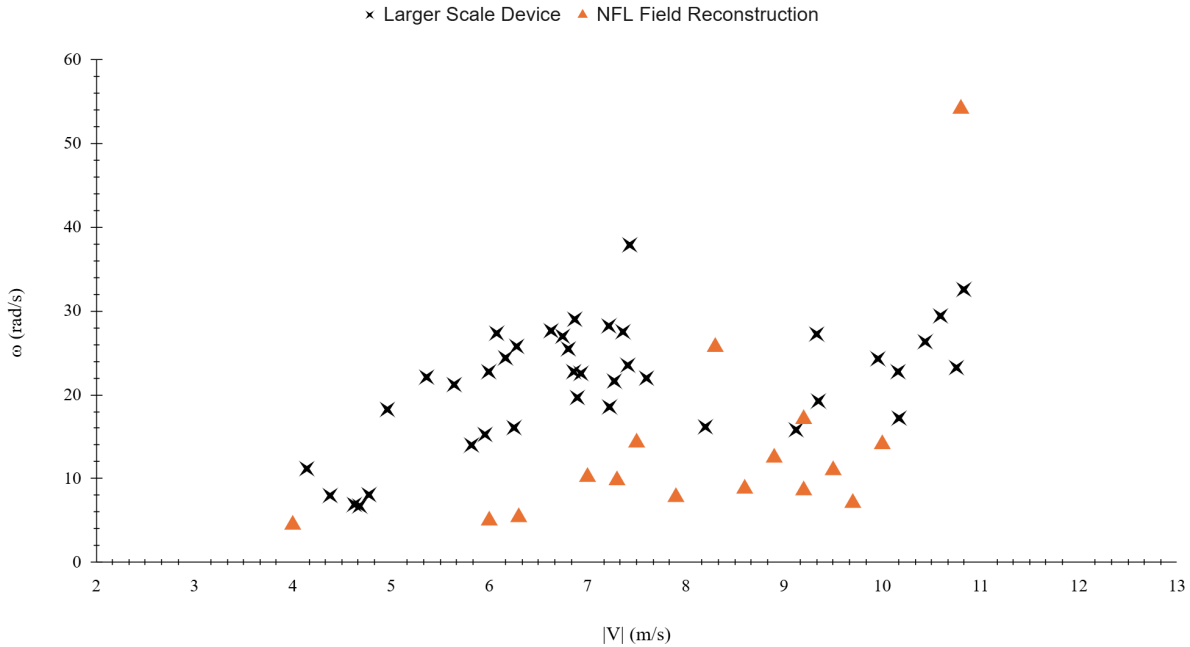


Figure 15: *Pre-Impact Rotational Velocities and Impact Linear Velocity Magnitude with Full Scale Model*

These specific conditions do not convey the full range of theoretically possible impact conditions. The entire area of the rectangle formed by $4 \text{ m/s} < |V| < 11.5 \text{ m/s}$ and $5 \text{ rad/s} < \omega < 60 \text{ rad/s}$ should be achievable. Each factor may be changed independently of the others to simulate different pre-impact conditions. For example, lowering the drop height of the track solely affects the pre-impact y direction (vertical) velocity. Because of this range and variability of pre-impact conditions, we believe that our design is a viable option for helmet companies to use to test H2G impact forces on football helmets.

Based on our results, the device was able to live up to the majority of the final specifications we installed for our design. The first specification we set out to achieve was a target linear resultant velocity range from 2.5 to 9 m/s and a target angular velocity range from 5

to 30 rad/s. The device was successful at obtaining these ranges as seen in Figure 10. The second specification was also completed successfully as our curved track design and ability to elevate the device provided independent control of horizontal and vertical velocity. In terms of our error, we hit specification 3 but fell short of specification 4. Our repeatability was strong as the standard deviation between identical tests was well under 2 m/s, but problems arose in regards to the error between theoretical and experimental values. Upon testing horizontal velocity, the device proved successful in maintaining an error under 5%. However, the average error for the device's vertical velocity in comparison to our theoretical values was slightly above 5%. Our reasoning for missing this goal is now understood as stated in the Testing section. Specifications 5 and 6 were both in regard to our device's ease of testing and operation, and both were met successfully. Finally, specification 7 was also met, as our product was made under our given budget since we relied so heavily on gravity to induce motion on the dummy. Overall, our device (pictured in Figure 16) was a success and proved as a large stepping stone in regards to further testing of head to ground impacts.



Figure 16: *Final Device*

Summary and Conclusions

This research project set out to design a device capable of simulating the full range of NFL head-to-ground impact velocities resulting in concussions for the provided data set. The goal was to cover a wide range of data with adjustability, and generate exceptionally reproducible impacts, with very little room for deviation on a test-to-test basis.

The purpose of this testing device would be to provide helmet manufacturers with a means to cheaply and accurately reproduce “whipping” impact conditions, a blow to the head that is not currently adequately prepared or accounted for in helmet design. Manufacturers, with

the help of this device and additional data from accelerometers, could design mechanisms to counter the unique blow that is caused by the whipping motion, and so better protect athletes.

Initially, our ideation process was ambitious. We aspired to simulate a wide range of complex impact conditions, including both linear and rotational components. However, as the project progressed, we came to understand the importance of simplification due to practical constraints such as budget, space, and available instrumentation. These limitations required us to scale down our vision while still maintaining the integrity and accuracy of our testing. Our final design focused on replicating critical head velocities at impact, using validated calculations and a repeatable testing process.

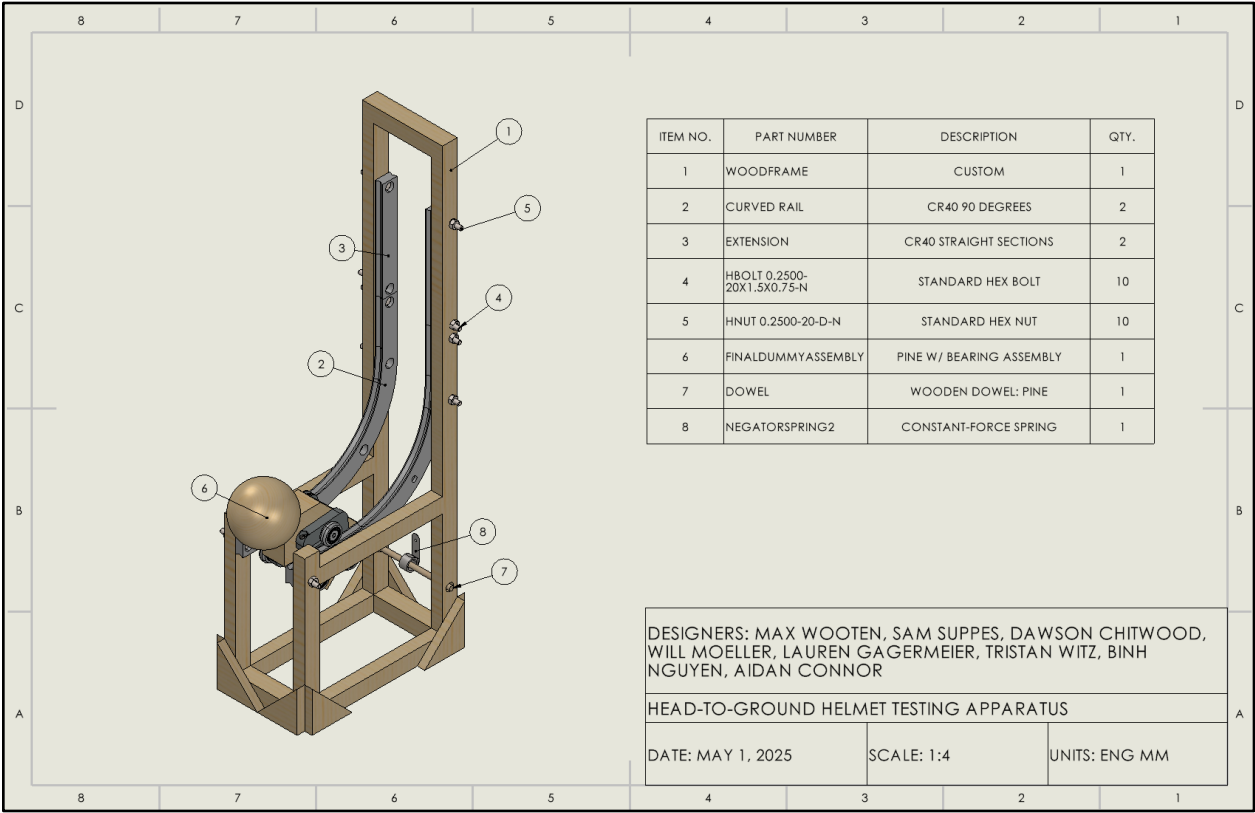
In pursuit of validation for the mathematical support of our device, a scale model was built on the exact specifications of the full device. This model was meant to prove the translation of our theory to practical application. Issues that arose in the construction of the model include materials procurement, fitment of the device, and the interface between the ultra-machined track and carriage system, and the much less so carpentry-built frame that it was situated on. An immediate issue that threatened to derail the design was warping of the wooden frame, causing binding and misalignment of the track, which allowed for almost no leeway in its connection with the carriage. This pinching was so great that at times we could not launch the dummy in any capacity from the track. Further iterations on the design provided bracing at the bottom edges of the wooden frame, and critical pre-tensioned steel cable mounts. These cables allowed for precise modifications to the frame alignment, which finally created the appropriate conditions for the track and carriage system.

In testing and collecting data samples we dealt with time constraints. Under our constraints we were able to collect data across 5 different track heights, 2 different drop heights,

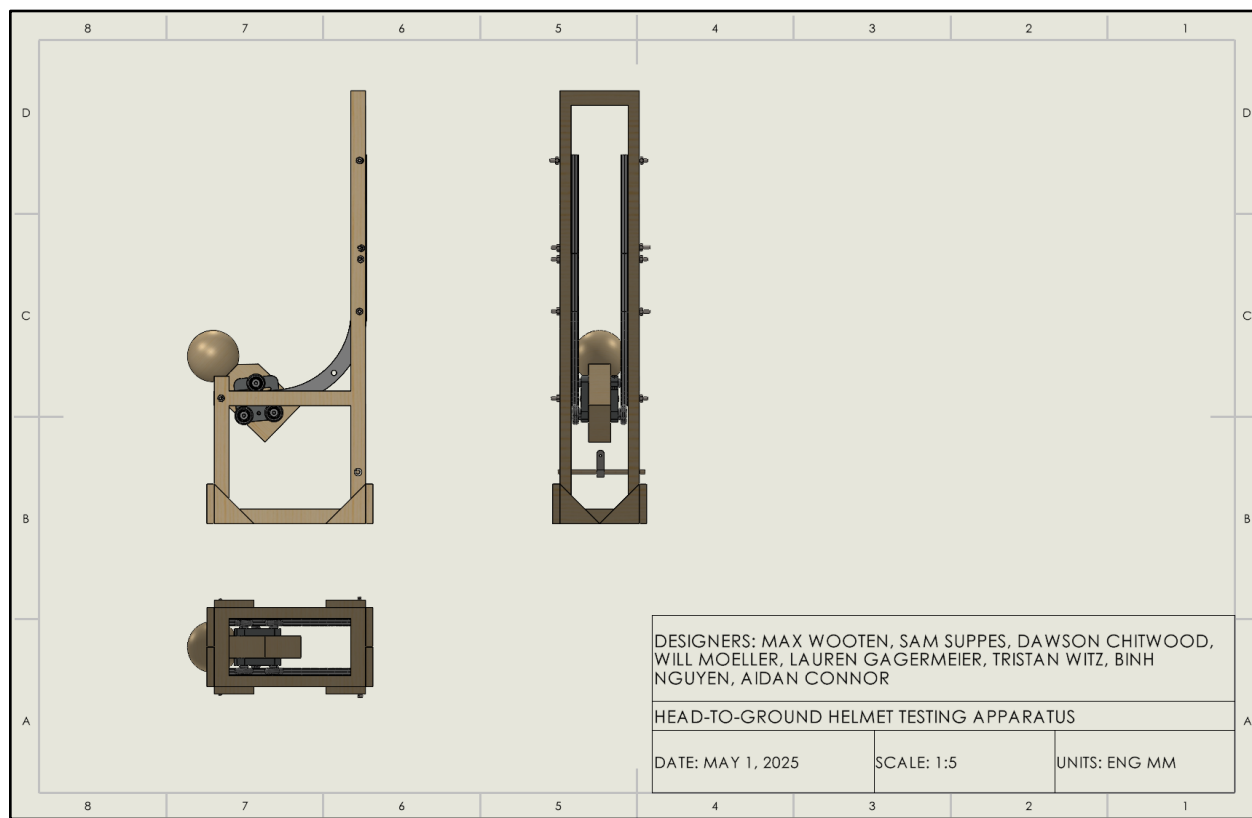
and used 3 different spring strengths. This provided us with a great sample data set, and using our theoretical values we can accurately predict that upon further testing we would be able to construct a complete data set that matches on field reconstructions. Our prototype demonstrated the ability to simulate the extremes, in resultant linear and rotational velocity of the desired data set, and within the given varying parameters, the exceptional level of flexibility, accuracy, and modification that was possible.

Ultimately, this project was successful in its pursuit of a design for our given problem. It created a device, which solved the problem given, and which did so inside all of the constraints provided. It was a simple, effective, and cheap answer to a pressing need. It was unsuccessful in a few of the processes taken by the team in pursuit of the design. If we were to further improve our device we would make improvements to the data capture methods, including the addition of accelerometers, manufacturable parts, and create a fully scaled model.

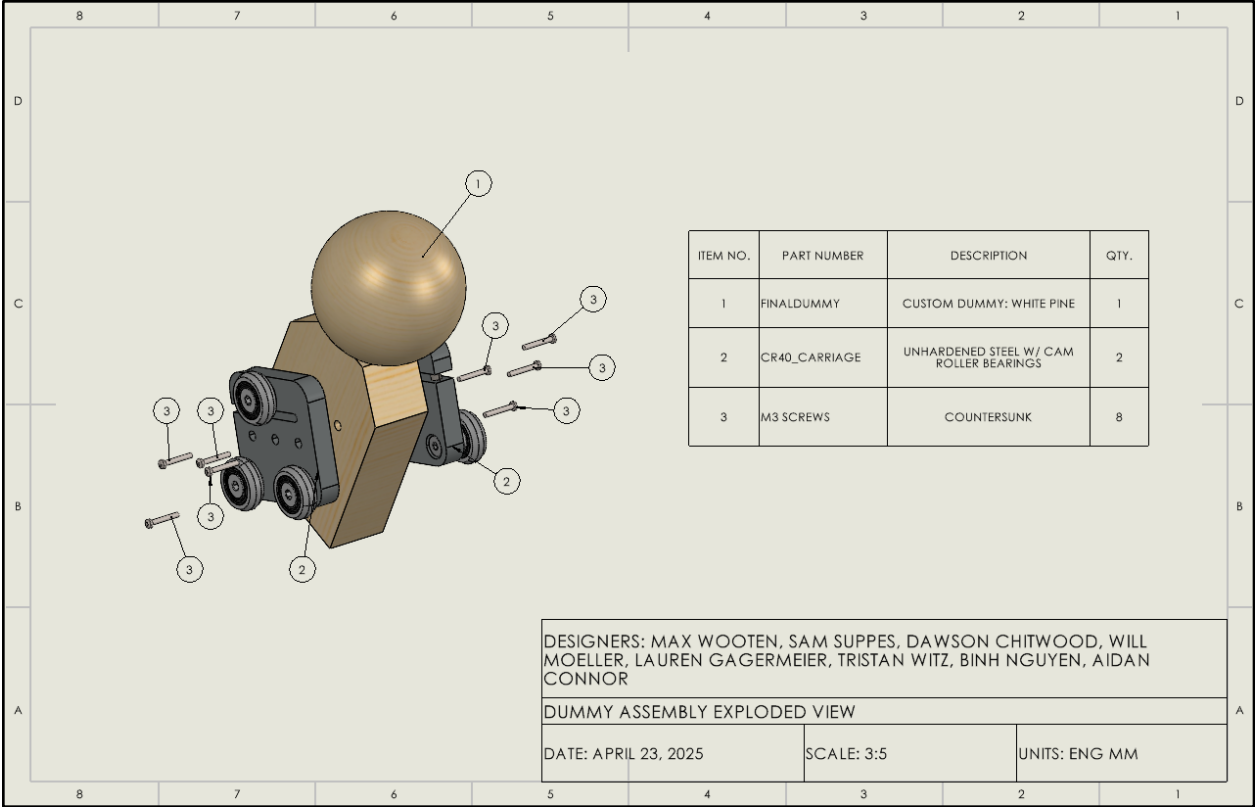
Appendix A: Drawings



Final Assembly

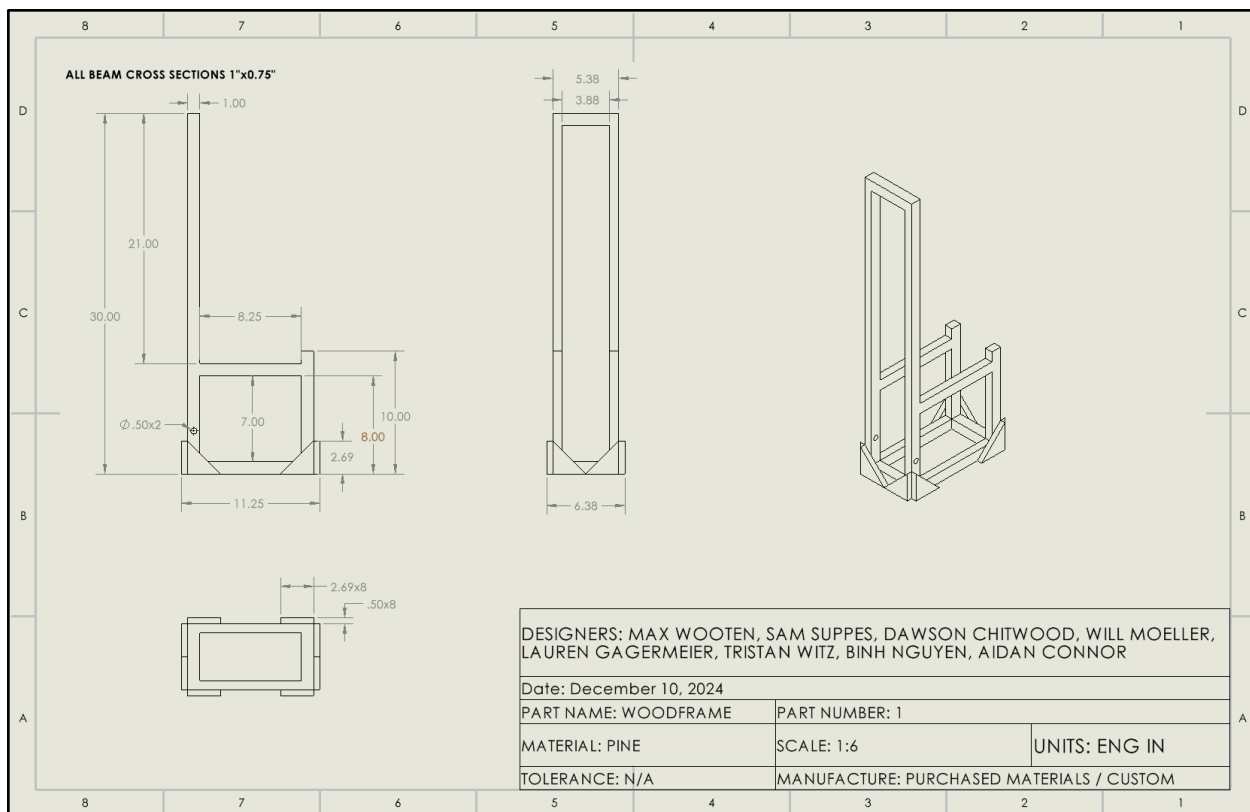


Projected Views of Final Assembly

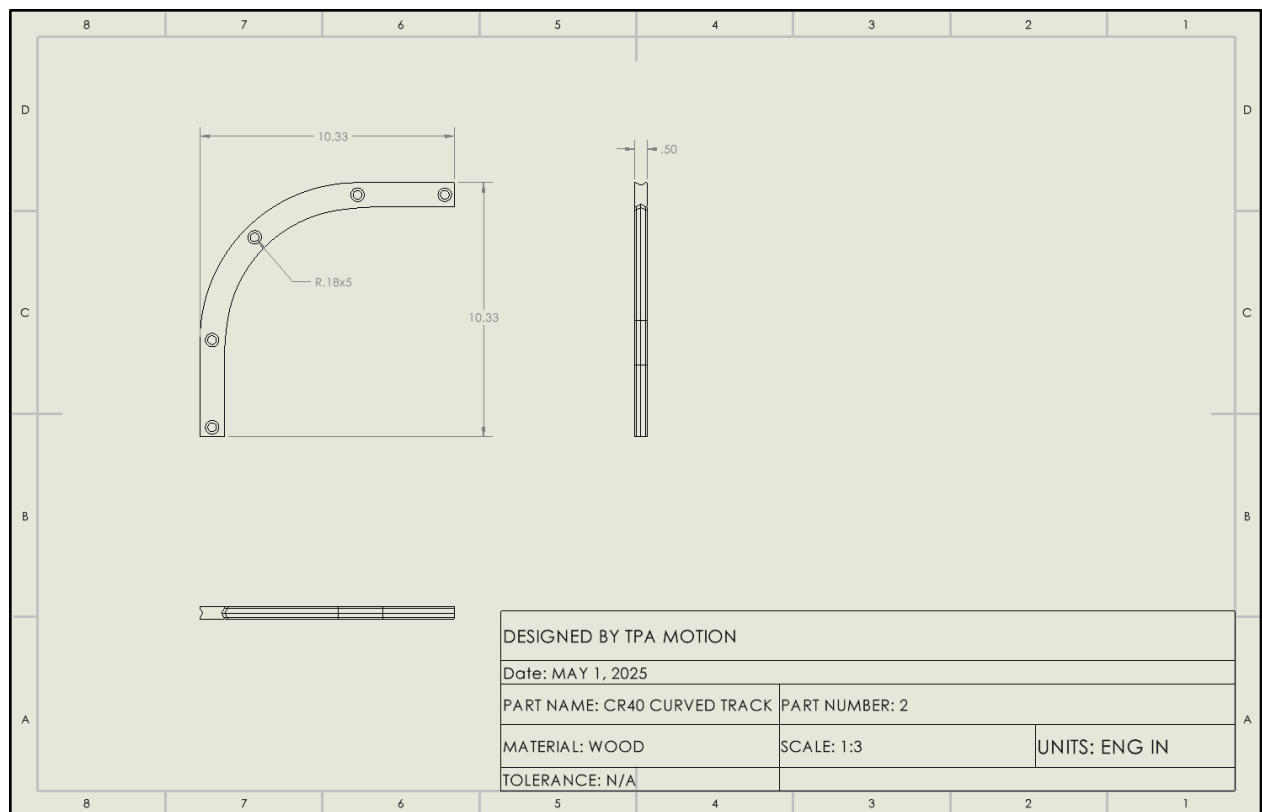


Exploded View: Final Dummy Assembly

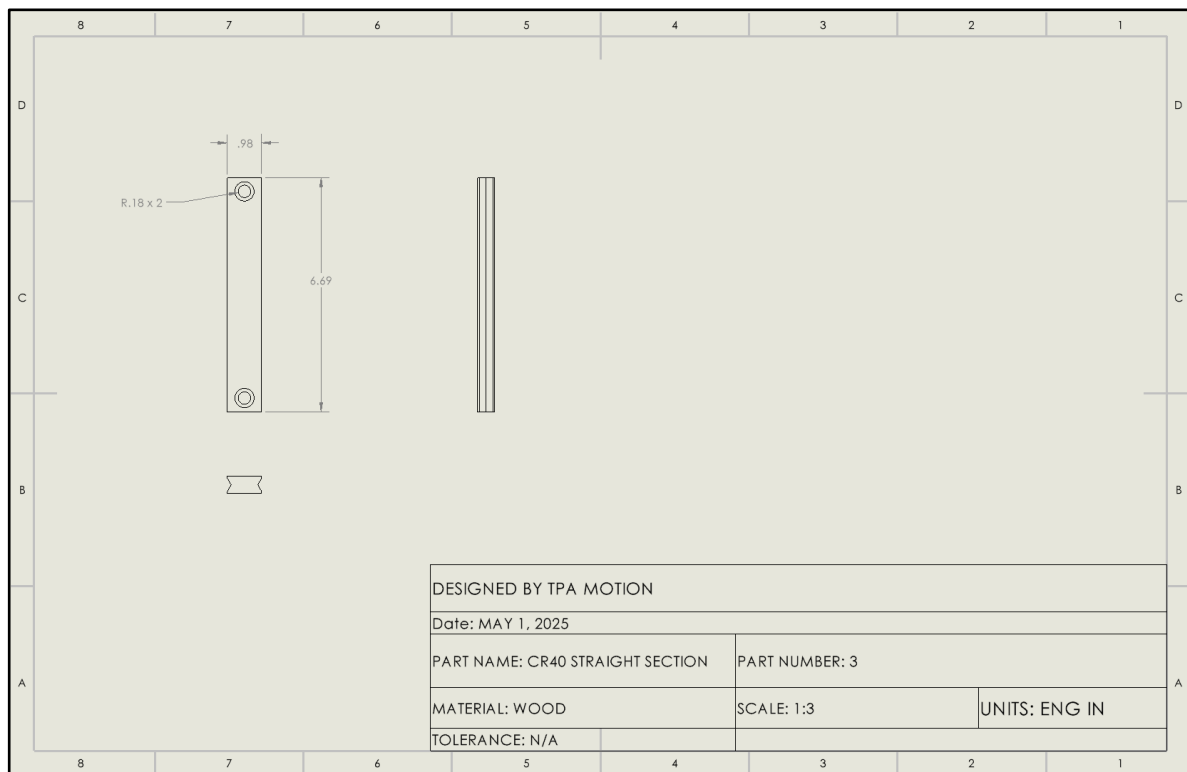
Final Dummy Drawing



Wood Frame Drawing



Curved Rail Drawing



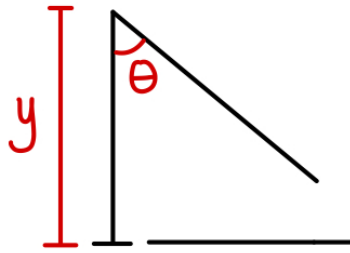
Rail Straight Extension Drawing

Appendix B: Bill of Materials

Part Number	Label Part	Description	Quantity	Unit Cost	Cost	Link
1	Track	CR40 90 Degree Sections	2	\$189.00	\$378.00	Here
2	Carriage	CR40 Carriages	2	\$182.77	\$365.54	Here
3	Extension	CR40 Straight Sections	2	\$127.75	\$255.50	Here
4	Latch	R4-10 MINI CONCEALED LEFT HANDED BOTTOM LEVER ROTARY LATCH	1	\$12.19	\$12.19	Here
5	Tensioner Kit	TooTaci Turnbuckle Wire Tensioner Kit with 100ft Stainless Steel Cable Wire Rope, 1/16 Vinyl Coated Steel Wire Cable, Turnbuckles for Cables Wire, Trellis Wire, Strings Light Hanging, Curtain Wire	1	\$27.99	\$27.99	Here
6	Crimping Tool	TooTaci Wire Cable Crimping Tool, Wire Rope Crimping Swager Crimper Up to 2.2mm (2/32 inch) with 3 Size Aluminum Double Barrel Ferrule Crimping Loop Sleeves 200 pcs	1	\$29.99	\$29.99	Here
7	Bag Balm	Bag Balm Vermont's Original for Cracked Hands, Dry Skin - Moisturizing Lotion Salve 8 Ounce - 2 Pack	1	\$15.07	\$15.07	Here
8	Spray Paint	Krylon COLORmaxx Spray Paint and Primer Gloss White (Pack of 1) and Gloss Black (Pack of 1)	1	\$20.19	\$20.19	Here
9	24.8 lb Spring	Constant-Force Spring 3000 Cycles, 52" Extended Length, 24.800 lbs. Load	1	\$27.53	\$27.53	Here
10	10.6 lb Spring	Constant-Force Spring 3000 Cycles, 40" Extended Length, 10.600 lbs. Load	1	\$16.03	\$16.03	Here
11	16.5 lb Spring	Constant-Force Spring 3000 Cycles, 50" Extended Length, 16.500 lbs. Load	1	\$21.34	\$21.34	Here
12	Frame Supplies	1" x 1" wood, bolts, nuts, washer, and wood glue to create frame for device	1	\$29.33	\$29.33	
13	Track Aligner	CR40 Alignment Tool	1	\$50.00	\$50.00	Here
14	Latch Pin	Hillman 1.25 Inch Silver Cotterless hitch pin Pin/Clip	1	\$5.98	\$5.98	Here

15	Foam Spacers	MEARCOOH Black Eva Foam,Premium Cosplay EVA Foam Sheet (1mm to 12mm,49"x13.5",1mm Thickness,for Cosplay Crafts DIY Projects	1	\$7.94	\$7.94	Here
16	Turnbuckle	Closed-Body Aluminum Closed-Body Aluminum Turnbuckle-Not for Lifting -Not for Lifting	2	\$2.30	\$4.60	Here
17	6.88 lb Spring	Constant-Force Spring 3000 Cycles, 28" Extended Length, 6.880 lbs. Load	1	\$5.64	\$5.64	Here
18	3.29 lb Spring	Constant-Force Spring 3000 Cycles, 30" Extended Length, 3.290 lbs. Load	1	\$11.97	\$11.97	Here
19	Hex Screw	18-8 Stainless Steel Hex Head Screw 1/4"-20 Thread Size, 7" Long	1	\$2.92	\$2.92	Here
20	Hex Nut	Alloy 20 Stainless Steel Hex Nut Ultra-Corrosion-Resistant, 1/4"-20 Thread Size	2	\$2.57	\$5.14	Here
21	Washer	Titanium Washer for 1/4" Screw Size, 0.265" ID, 0.75" OD	4	\$1.57	\$6.28	Here
				Total Cost	\$1,299. 17	

Appendix C: Initial Design Calculations



$$g = 9.8 \text{ m/s}^2$$

$$\theta = 45^\circ$$

$$v_R = 8 \text{ m/s}$$

$$mgh = \frac{1}{2} m v_R^2$$

$$v_R = \sqrt{2gy}$$

$$8 = \sqrt{2(9.8)y}$$

$$y = 3.26 \text{ m}$$

Appendix D: Testing Results

<u>Test Number</u>	<u>Spring Strength (N)</u>	<u>Drop Height (m)</u>	<u>Track Height (mm)</u>	<u>X velocity</u>	<u>Y velocity</u>	<u>Rotational Velocity (rad/s)</u>	<u> V (m/s)</u>
1	0.00	0.16	410.0	2.47	2.18	24.80	3.29
2	0.00	0.16	410.0	2.36	2.18	22.80	3.21
3	0.00	0.16	410.0	2.48	2.21	24.10	3.32
4	0.00	0.16	359.2	2.35	2.20	24.60	3.21
5	0.00	0.16	359.2	2.35	2.02	22.70	3.09
6	0.00	0.16	359.2	2.30	2.28	32.00	3.24
7	0.00	0.16	308.4	1.98	2.20	28.90	2.96
8	0.00	0.16	308.4	2.25	2.42	27.20	3.31
9	0.00	0.16	308.4	2.08	2.33	26.10	3.12
10	0.00	0.16	257.6	2.02	2.32	33.40	3.07
11	0.00	0.16	257.6	1.73	2.06	20.40	2.69
12	0.00	0.16	257.6	1.88	2.17	10.99	2.88
13	0.00	0.16	206.8	1.54	1.97	11.30	2.50
14	0.00	0.16	206.8	1.64	2.20	10.01	2.74
15	0.00	0.16	206.8	1.67	2.11	12.25	2.69
16	30.60	0.16	410.0	4.64	2.16	25.10	5.12
17	30.60	0.16	410.0	4.78	1.94	24.90	5.16
18	30.60	0.16	410.0	5.06	2.50	26.40	5.64
19	30.60	0.16	359.2	4.50	2.42	28.90	5.11
20	30.60	0.16	359.2	4.82	2.44	27.80	5.40
21	30.60	0.16	359.2	4.60	2.50	24.20	5.23
22	30.60	0.16	308.4	4.33	2.45	16.31	4.98
23	30.60	0.16	308.4	4.10	2.12	14.98	4.62
24	30.60	0.16	308.4	4.10	2.22	16.94	4.66
25	30.60	0.16	257.6	3.92	2.38	15.89	4.59
26	30.60	0.16	257.6	3.73	2.09	15.54	4.28

27	30.60	0.16	257.6	3.86	2.33	14.35	4.51
28	30.60	0.16	206.8	3.61	2.45	14.84	4.36
29	30.60	0.16	206.8	3.59	2.36	12.95	4.30
30	30.60	0.16	206.8	3.52	2.48	14.21	4.30
31	14.63	0.16	410.0	4.06	2.34	27.27	4.68
32	14.63	0.16	410.0	4.00	2.17	23.17	4.55
33	14.63	0.16	410.0	4.24	2.18	22.75	4.77
34	14.63	0.16	359.2	3.65	2.41	20.37	4.38
35	14.63	0.16	359.2	3.77	2.51	23.16	4.53
36	14.63	0.16	359.2	3.72	2.66	24.71	4.58
37	14.63	0.16	308.4	3.24	2.32	21.07	3.98
38	14.63	0.16	308.4	3.43	2.52	22.54	4.25
39	14.63	0.16	308.4	3.43	2.42	20.02	4.19
40	14.63	0.16	257.6	3.07	2.47	24.01	3.94
41	14.63	0.16	257.6	3.22	2.40	20.51	4.02
42	14.63	0.16	257.6	2.90	2.18	21.77	3.63
43	14.63	0.16	206.8	2.68	2.58	19.11	3.72
44	14.63	0.16	206.8	2.54	2.12	16.38	3.31
45	14.63	0.16	206.8	2.71	2.40	19.25	3.62
46	47.15	0.16	410.0	5.83	2.53	44.87	6.36
47	47.15	0.16	410.0	5.39	2.58	32.83	5.97
48	47.15	0.16	410.0	5.12	1.90	35.91	5.46
49	47.15	0.16	359.2	4.87	1.91	26.88	5.23
50	47.15	0.16	359.2	5.02	1.90	34.93	5.36
51	47.15	0.16	359.2	5.17	1.93	25.20	5.52
52	47.15	0.16	308.4	4.83	2.10	30.94	5.27
53	47.15	0.16	308.4	4.80	1.92	25.06	5.17
54	47.15	0.16	308.4	4.58	1.88	26.90	4.95
55	47.15	0.16	257.6	4.22	1.81	26.00	4.60
56	47.15	0.16	257.6	4.48	1.94	25.60	4.88
57	47.15	0.16	257.6	4.35	2.17	25.70	4.86
58	47.15	0.16	206.8	4.21	2.35	29.20	4.82

59	47.15	0.16	206.8	3.81	2.22	27.90	4.41
60	47.15	0.16	206.8	4.00	2.04	24.90	4.49
61	0.00	0.41	410.0	2.51	3.08	-23.52	3.98
62	0.00	0.41	359.2	2.45	3.28	-19.67	4.09
63	0.00	0.41	308.4	2.25	3.00	-21.63	3.75
64	0.00	0.41	257.6	2.14	3.43	-22.54	4.05
65	0.00	0.41	206.8	2.01	3.30	-22.75	3.86
66	14.63	0.41	410.0	3.47	2.94	-21.98	4.55
67	14.63	0.41	359.2	3.82	3.06	-27.51	4.89
68	14.63	0.41	308.4	3.70	3.02	-28.21	4.78
69	14.63	0.41	257.6	3.34	2.93	-18.55	4.44
70	14.63	0.41	206.8	3.14	3.28	-16.17	4.54
71	30.60	0.41	410.0	4.96	3.25	-29.40	5.93
72	30.60	0.41	359.2	4.68	2.98	-24.29	5.55
73	30.60	0.41	308.4	4.11	2.81	-26.32	4.98
74	30.60	0.41	257.6	3.93	3.24	-15.82	5.09
75	30.60	0.41	206.8	3.46	2.99	-19.25	4.57
76	47.15	0.41	410.0	5.61	2.99	-32.55	6.36
77	47.15	0.41	359.2	4.99	2.71	-23.24	5.68
78	47.15	0.41	308.4	4.85	2.64	-22.75	5.52
79	47.15	0.41	257.6	4.01	2.66	-17.22	4.82
80	47.15	0.41	206.8	4.42	3.10	-27.23	5.39

Appendix E: Bibliography

Bibliography

Kent, R., Forman, J., Bailey, A. M., Funk, J., Sherwood, C., Crandall, J., Arbogast, K. B., Myers, B. (2019). The biomechanics of concussive helmet-to-ground impacts in the National Football league. *Journal of Biomechanics*, 99, 0021-9290.

https://www.sciencedirect.com/science/article/pii/S0021929019308085?casa_token=NK1

Kent, R. (2024). *Head to Ground test device*.

<https://canvas.its.virginia.edu/courses/115860/files/folder/Project%20Descriptions?preview=9420534>

Kent, R., Forman, J., Bailey, A. *et al.* Surface Contact Features, Impact Obliquity, and Preimpact Rotational Motion in Concussive Helmet-to-Ground Impacts: Assessment *via* a New Impact Test Device. *Ann Biomed Eng* 48, 2639–2651 (2020).

<https://doi.org/10.1007/s10439-020-02621-x>

Lessley, D. J., Kent, R. W., Cormier, J. M., Sherwood, C. P., Funk, J. R., Crandall, J. R., Myers, B. S., & Arbogast, K. B. (2020). Position-Specific Circumstances of Concussions in the NFL: Toward the Development of Position-Specific Helmets. *Annals of biomedical engineering*, 48(11), 2542–2554.

<https://doi.org/10.1007/s10439-020-02657-z>